Computational Study of a Quadcopter Propeller in Hover at High Altitude

Andres M. Pérez G.[1] Omar D. López.[2]
Department of Mechanical Engineering, Universidad de los Andes, Bogotá, 1117711

and
Jaime Escobar.[3]
ADVECTOR, Chia, Colombia, 250001

Quadcopter are the main platform for UAV, the use of this technology is growing fast for different industries as agriculture, mining and oil and gas. CFD has been used to model the wake of propellers, the Spalart Allmaras and k-ω turbulence models were used to simulate a propeller at hover. Both models predicts the wake induced for the propeller, and the behavior of lift and torque coefficients for the propeller. For validation the results of thrust and torque form the models were compared with experimental measurements of flying test. The wake, forces, torque pressure and velocities with the two models are similar; the main difference found was the turbulent viscosity field.

Nomenclature

SA	=	Spalart Allmaras turbulence model
a	=	cylinder diameter
C_l	=	lift coefficient
C_m	=	torque coefficient
$\vec{v}_r$	=	relative velocity
$\vec{\omega}$	=	rotational velocity

I. Introduction

NOWDAYS quadcopters are the preferable platform used for unmanned aerial vehicle (UAV) for commercial and industrial use (1). Agriculture is using drones more than any other industry, so far, followed by construction. Drones mapped 3 million acres of land from April to august 2016, (94% using quadcopters) But the fastest growth in adoption of drones is seen in mining, inspection and oil and gas (1). The increasing use of quadcopters is due to an easier control in flight for drone operators and because allows for a rapid takeoff. Meanwhile the advantages of a quadcopter over other vertical takeoff and landing (VTOL) UAV's are: 1) quadrotors do not require complex mechanical control, instead it uses electrical brushless motors, making variations in motor speed for vehicle control. 2) The use of four rotors ensures that the rotors are smaller than the equivalent main rotor on a helicopter (2).

The research community has been studying quadcopters in the last years, most of them developing the control system for these vehicles, but the aerodynamic effects of the rotorcraft vehicles have been often ignored (2). The wake of a rotorcraft has a significant effect on the overall flow field and on the performance of the vehicle (3). The wake is characterized by induced velocities and regions with intense vortical flow which interact with rotor blades and fuselages (3). In Computational Fluid Dynamics (CFD) analyses of rotorcraft it is desired to model the rotor wake and tip vortices as accurately as possible (3). Turbulence modeling plays a major role in CFD of rotorcraft to resolve the details of the tip vortices, therefore the turbulence model has an effect in both near and far flow field predicted (3).

[1] Postgraduate student, Mechanical Engineering Department, Universidad de los Andes, Bogotá, Colombia.
[2] Associate professor, Mechanical Engineering Department, Universidad de los Andes, Bogotá, Colombia.
[3] Research and development, ADVECTOR, Chia, Colombia.

Turbulence models like Spalart-Allmaras or k-ω have been wide used to model external flows over airfoils, wings and rotors (3). In wall-bounded flows the vorticity and the strain are of similar magnitude, but this is not true in a vortex core where the vorticity is high, but the strain is low. In these models the turbulence production term is based on the velocity gradient (3). The dependence of the production term on vorticity is problematic, then some modification have been proposed to existing models, in order to include the effects of rotation (3). Turbulence models with rotation and curvature terms do not suffer of this problem, for example the full Reynolds Stress turbulence models. But these models are still computational expensive (3). Rotation and curvature corrections have been developed for different models like the Spalart-Almaras model achieving satisfactory results.

Postdam M. and Pulliam T. (3) studied the influence of turbulence modelling in the vertical wake of rotorcraft simulations, Baldwin-Bart and Spalart-allmaras models were used including some modifications such as turning off the production source term. It was found a problem with the dependence of vorticity of the eddy viscosity production term, but this problem is reduced using modifications to the turbulence model such as turning off production terms and/or rotation and curvature corrections. Also discrepancies were observed between isolated hover performance predictions using steady-state and moving grid with unsteady formulations.

Duraisamy K. and Baeder J. D. (4) used a high-resolution Reynolds-averaged Navier–Stokes (RANS) solver to study the evolution of tip vortices from rotary blades, computations were performed using a modified version of the compressible RANS code TURNS, the discretization of the inviscid terms were computed using the fifth order WENO upwind scheme. The viscous terms were discretized using the second order central differencing. The Spalart-Allmaras turbulence model with rotational correction was used to close the RANS equations. It was found that practical RANS simulations of tip vortex formation and evolution suffer from: numerical diffusion, due from inaccuracies in the discretization of the convective term, and inaccurate turbulence modeling, it is a result of the unavailability of a perfect closure model to the RANS equations. But the error from numerical diffusion was reduced by the use of proper grid resolution and high-order accurate numerical schemes and reliable solutions can be obtained by adding a simple rotational correction to the production term in the Spalart-Allmaras turbulence model.

Doerffer P. and Szulc O. (5) performed numerical simulations or a rotor with the code SPARC developed at the University of Karlsruhe. This code solves numerically compressible, mass-weighted, Reynolds-averaged Navier-Stokes (RANS) equations with the Spalart-Allmaras turbulence model. The algorithm uses a semi-discrete approach, utilizing a finite-volume, density-based formulation for spatial discretization and explicit Runge-Kutta type method for integration in time. It was found that the RANS method using structured grids is known to be very dissipative and to produce a tip vortex that is diffused very soon, however, the tip vortex descent and contraction rates were accurately predicted by the method.

Pandey K. M. et al. (6) modeled the flow around an isolated helicopter rotor at 800 rpm during hovering flight conditions, the Multiple Reference Frame (MRF) method with standard viscous k-ε turbulent flow model was used. At a speed around 800 RPM wake formation and tip vorticity increases, thus affecting the lift of the helicopter resulting in unsteady hover, however the study does not shows figures of vortices using a criterion for the identification of flow field vortices.

Yoon S., Chaderjian N. M., Pulliam T. H., and Holst T. L., (7) compared the solution from RANS and Laminar Off-Body (LOB) models, using the OVERFLOW CFD. For off-body grids two approaches were used, the DES approach assumes that the wall-parallel grid spacing, Δ, exceeds the thickness of the boundary layer so that the RANS model remains active near solid surfaces, and the LOB approximation, which does not account for turbulence production, dissipation or diffusion in the lower wake (off-body grids). It was found that the choice of turbulence models for off-body grids affects the accuracy of solutions, if the RANS model is used for both near and off body grids, it underpredicts the figure of merit, if it is compared to the LOB model results. The pressure on the upper surface of the LOB model is lower than that of the RANS model. Higher pressure of the RANS model on the upper surface results in an increase in torque and a decrease in thrust. Thus, the figure of merit, that is a ratio of thrust over torque, is lower for the RANS than for the LOB model.

Gomez S., Gilkey L. N., Kaiser B. E., and Poroseva S. V., (8) analyzed the effects that a bio-inspired blade shape has on the size and structure of a tip vortex, two turbulence models were used in simulations: Menter's Shear Stress Transport (SST) version of the k- ω model and the Spalart-Allmaras (SA) model. Differences in the results produced with the two models for the fixed blade setting were found to be

negligible. The rectangular blade generates a vortex with higher values of turbulence kinetic energy than the bio-inspired blade does, and the vorticity magnitude decreases more rapidly behind the bio-inspired blade.

Lazaro C. M. and Poroseva S. V., (9) studied the effect of a number of blades on the flow structure around a ducted propeller and propeller designs with and without duct are compared by conducting flow simulations. Computations were conducted with Menter's Shear Stress Transport (SST) version of the k-ω turbulence model. When comparing with unducted propellers, ducted propellers develop a less intense, but more complicated wake structure, however, unducted propellers showed to have higher thrust coefficient and figure of merit than ducted ones.

The quad-rotor Araknos V2 was used for the experimental study (Fig.2). The Araknos V2 was designed and manufactured by Advector Unmaned Systems in Colombia. It is a remotely piloted aircraft system (RPAS) developed for civil application such as surveying, agriculture, and inspection. The aircraft is capable of fully automatic flight, has a standard empty mass of 1,700 gr, and it is able to carry a weight of 700 gr for up to 15 minutes. To understand how the aerodynamic effects of rotorcraft impact the performance of the vehicle, it is important to execute a CFD study to the rotor wake. This paper presents the results of two turbulence models typically used on CFD simulations of external flow at moderate and high Reynolds numbers. The study also wants to perform simulations with the air conditions at high altitudes common flying conditions for the operation of the Araknos.

Figure 1. CAD model of the propeller.

II. Computational Methodology

A. Geometry and Computational Domain

The actual rotor blade installed in the quad-rotor model Araknos V2 of the Colombian company ADVECTOR is used for this study. A 3D scanning was performed to obtain a CAD of the propeller see (Fig. 1). The diameter of the propeller (DP) is 360mm, the root chord is 20.77mm, the tail chord is 4.33mm, the chord at 75% of span is 25.31mm. The computational domain is a vertical cylinder, with 3.3 and 7 DP length, the propeller is centered in the domain and at 2.7 PD from the upper surface. The mesh is an unstructured grid of tetrahedral elements but with a refined grid of pyramidal elements near the propeller. The number of elements of the grid was varied from 800.000 to 16.000.000.

B. Numerical Methods and Boundary Conditions

The present study was performed in steady state using the multiple reference frame MRF model. The conservative equations for a MRF are equations (1) and (2) (10):

$$\frac{\partial \rho}{\partial t} + \nabla \cdot \rho \vec{v}_r = 0 \tag{1}$$

$$\frac{\partial \rho \vec{v}}{\partial t} + \nabla \cdot (\rho \vec{v}_r \vec{v}) + \rho(\vec{\omega} \times \vec{v}) = -\nabla p + \nabla \bar{\bar{\tau}} + \vec{F} \tag{2}$$

Where $\vec{v}_r$ is the relative velocity, $\vec{\omega}$ is the rotational velocity, and in this case the Coriolis and centripetal accelerations are into a single term $\vec{\omega} \times \vec{v}$. Many problems permit the entire computational domain to be referred to as a single rotating reference frame SRF. Steady-state solutions are possible in SRF models if suitable boundary conditions are prescribed (10). For all the simulations the boundary conditions for the upper and lateral surface of the cylinder were set as pressure inlet with a gauge pressure of 0pa, the lower surface was set as a pressure outlet with a gauge pressure of 0pa, and the propeller boundary was set as a wall. As a result of this adjustment, the movement of the flow is because of the rotation of the propeller.

All simulations were implemented in the CFD software ANSYS FLUENT 17.0. The pressure-velocity solver SIMPLE was used, with second order upwind discretization for convective and diffusive terms. The simulations were performed increasing the rotational velocity with small discrete steps starting with 1 rpm to reach 6547 rpm, though the results presented here are for 5221 and 6547 rpm, for each step of velocity the

model was running till the variation of residuals was very small, the convergence criteria were adjusted to 1×10^{-5}. The model was adjusted to the air conditions of the experimental test, with the density of the air of $0.877\ kg/m^3$, the viscosity was calculated using Sutherland's equation for the temperature of 24 °C which means a viscosity of $1.856\ kg/m-s$. The iterations were different for each time step, but for a complete simulation were necessary 75000 iterations.

C. Turbulence Models

Two different turbulent models were tested in this study, the Spalar Allmaras and the $k-\omega$ models both with curvature correction.

The Spalart-Allmaras model is a relatively simple one-equation model that solves a modeled transport equation for the kinematic eddy (turbulent) viscosity. The Spalart-Allmaras model was designed specifically for aerospace applications involving wall-bounded flows and has been shown to give good results for boundary layers subjected to adverse pressure gradients. It is also gaining popularity for turbomachinery applications (10). The Spalart Allmaras model solves a transport equation for the turbulent kinematic viscosity. This model does not solves the turbulent kinetic energy (11), then the last term of the Boussinesq approximation is ignored, the Boussinesq approach is used to model the Reynolds stresses through the velocity gradient. More detail about the model, equations and constants can be found in reference (11).

For the Spalart-Allmaras model, in the reference (12) was developed a modification of the production term to take streamline curvature and system rotation effects into account, this is an empirical function which multiplies the production term for the Spalart-Allmaras one-equation turbulence model. More information can be found at reference (12).

The standard $k-\omega$ model is an empirical model based on model transport equations for the turbulence kinetic energy k and the specific dissipation rate ω. The model predicts free shear flow spreading rates that are in close agreement with measurements for far wakes, mixing layers, and plane, round, and radial jets, and is thus applicable to wall-bounded flows and free shear flows (10). All the equation of the model and the approximation used to model diffusion, turbulence production and dissipation, as the model constants can be found at reference (13). The shear stress transport SST $k-\omega$ model is similar to the standard $k-\omega$ model but includes the following refinements: a blending function activates $k-\omega$ model in the near-wall region, and away from the surface this function activates the $k-\epsilon$ model (10). The SST model incorporates a damped cross-diffusion derivative term in the ω equation (10). The definition of the turbulent viscosity is modified to account for the transport of the turbulent shear stress (10). These features make this model more accurate and reliable for a wider class of flows (10). A detailed description of the model can be found at reference (14).

One drawback of the $k-\omega$ model is that this model is not sensitive to streamline curvature and system rotation. As for the Spalart Allamaras model, a modification to the turbulence production term is available to sensitize the model to the effects of this these flows. The multiplier function for this model is similar to the used for Spallart Allmaras model, but the equations of some terms and the constants are different, for more details see reference (15).

Figure 2. Multirotor Araknos V2.

III. Experimental Methodology

The objectives of the flight tests were to measure current consumption, voltage gradient, and rotational speed of the propellers for four different thrust settings. A total of four flights were conducted maintaining a hovering position at an altitude over 15 meters above ground level (AGL) to assure out-of-ground-effect. All of these flights were conducted at an atmospheric pressure of 748 hPa and an average atmospheric temperature of 24ºC.

The Araknos V2 was used with its default configuration given in the "Flight Manual", with the only change being the removal of the bottom cover, setting a standard empty weight of 17.825N, including the weight of the battery being used. The variable of these tests was the weight of the payload, varying with the placement of different amounts of battery packs held by Velcro strips at the bottom of the aircraft, resulting in four different take-off weights of 17.825N, 22.543N, 26.928, and 31.392N for test 1, 2, 3 and 4 respectively. Power for the motors and avionics were supplied only from one battery while the other batteries were used as ballast. These flights were monitored using the software Mission Planner, which provided real-time information on battery voltage and control output to the engines.

Flight data collected from the IMU, barometer, voltage and current sensor, and control output were recorder by the autopilot and downloaded for analysis. The data was reduced to discard information acquired during takeoff, climb, descent, and landing maneuvers. The data of rotational speed and electrical power recorded during hovering flight was analyzed, the other magnitudes were calculated from the records.

IV. Results

A grid convergence analysis was performed using 6 different meshes with total number of elements varying from 0.8 to 16 million cells. Total torque and thrust were used as convergence criteria at 5221rpm. It was found that for an increase of the number of elements from 9.6 to 16.5 million, the change in the force predicted was 0.2% while for the moment the change was of 0.03% see figure 3, it was concluded that the mesh with 9.6 million cells was sufficient. Details of the mesh can be seen in figure 4, with a detailed view of the elements near the propeller´s wall. The maximum volume of the cells was $9.27\times10^{-7}\ m^3$, while the minimum was $7.93\times10^{-14}\ m^3$, the maximum face area was $2.23\times10^{-4}\ m^2$ and the minimum was $5.43\times10^{-10}\ m^2$.

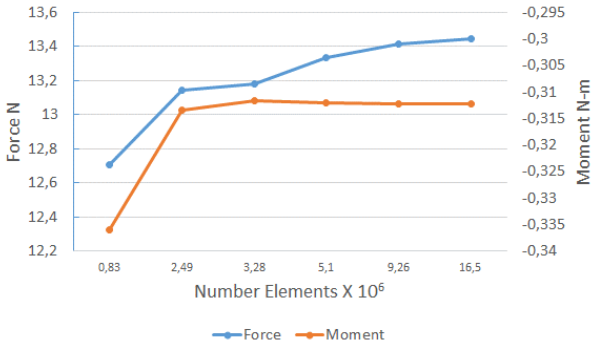

Figure 3. Mesh convergence, force and moment on the propeller.

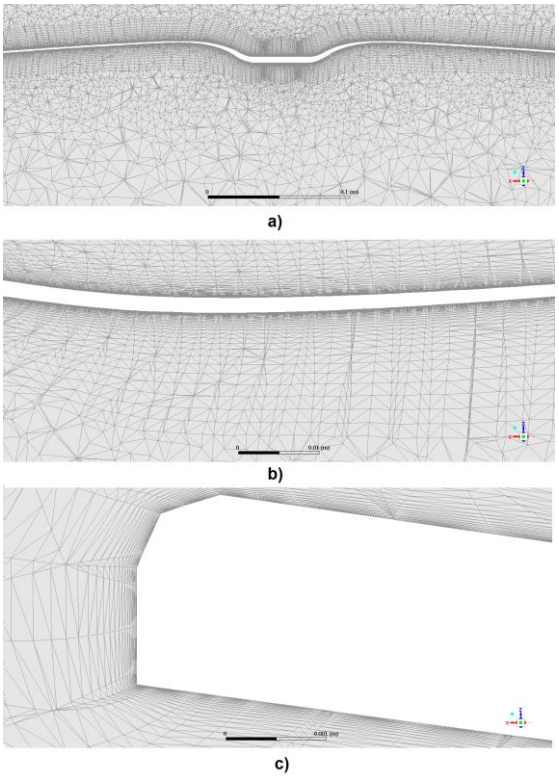

Figure 4. Mesh. a) general mesh around the propeller, b) pyramidal elements near wall, c) detail of the mesh at propeller tail.

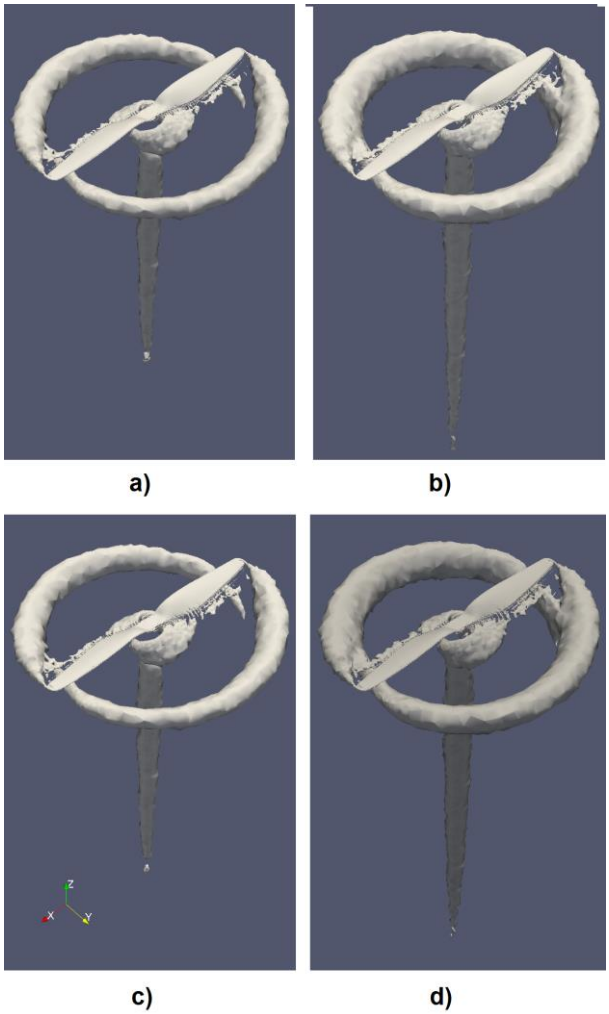

Figure 5. Contours of Q-Criterion= 25000. a) SA 5221RPM, b) SA 6547RPM, c) $k-\omega$ 5221RPM, d) $k-\omega$ 6547RPM.

Figure 5 shows the iso-surfaces of Q-Criterion of the propeller, left shows the wake for 5221 rpm while in right the wakes for 6547 rpm. Both models show stronger vortex for a higher velocity, the tip vortices are bigger for a higher velocity, also the central vortex is longer in the case of 6547rpm. The differences of the predicted wake for both models are not clear.

Figure 6 are the iso-surfaces of Q-Criterion and the turbulent viscosity on a symmetrical vertical plane through the center of the computational domain. The results of the models are similar to the results showing in reference (7). With SA model the turbulent viscosity is the same for both velocities while $k-\omega$ model shows that for a higher velocity, the turbulent viscosity is also higher especially at the far wake.

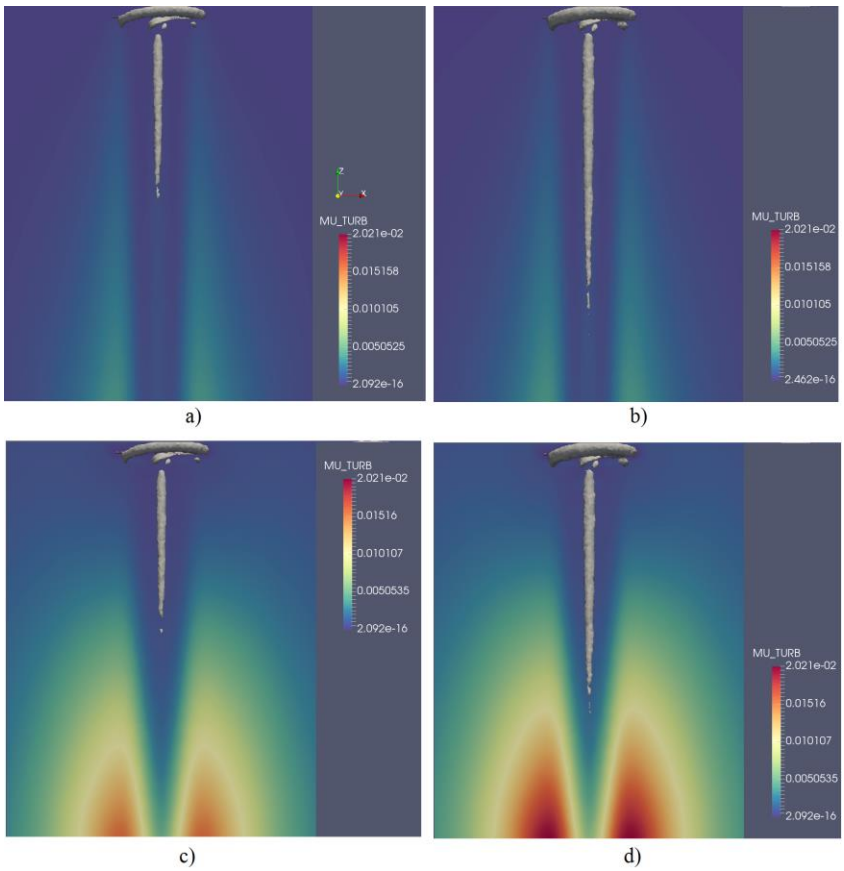

Figure 6. Turbulent viscosity and contours of Q-Criterion= 25000. a) SA 5221RPM, b) SA 6547RPM, c) $k-\omega$ 5221RPM, d) $k-\omega$ 6547RPM.

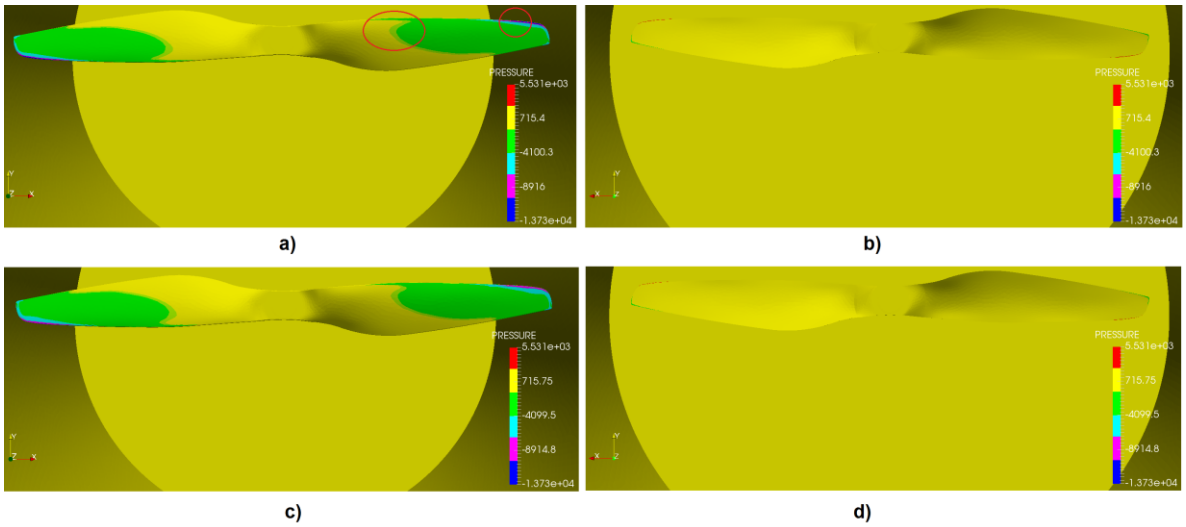

Figure 7. Pressure contours for 6547RPM, Pa. a) SA upper face, b) SA lower face, c) $k-\omega$ upper face, d) $k-\omega$ lower face.

Figure 7 shows the contours of pressure for the upper and lower surfaces of the propeller. As expected the pressure is lower at the upper surface of the propeller. The pressure contours of the upper surface for both turbulent models are quite similar but the $k-\omega$ contours are slightly higher than SA contours.

Figure 8 and 9 show the lift and torque coefficients for $k-\omega$ and SA models as function of the propeller rpm. It is clear a quadratic dependence of angular velocity, which is in agreement with the theory for propellers. For velocities over 3000 rpm the $k-\omega$ Cl is slightly higher than SA predictions of them.

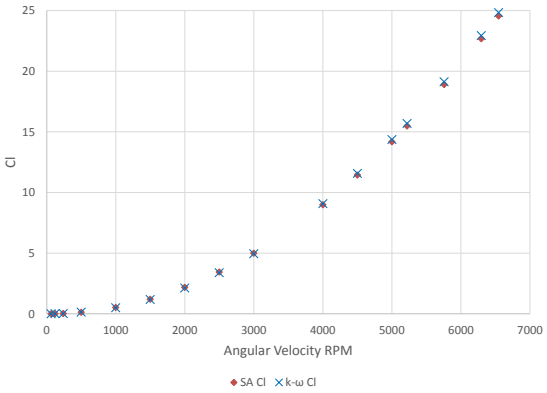

Figure 8. Lift coefficient Cl..

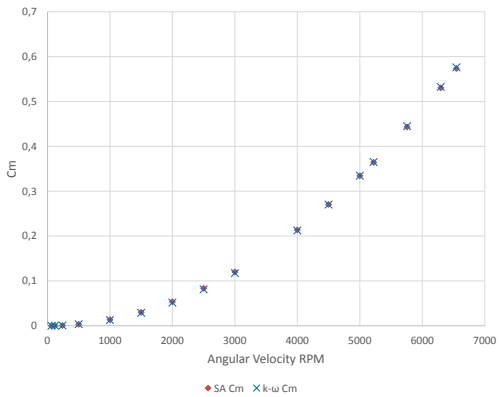

Figure 9. Torque coefficient Cm

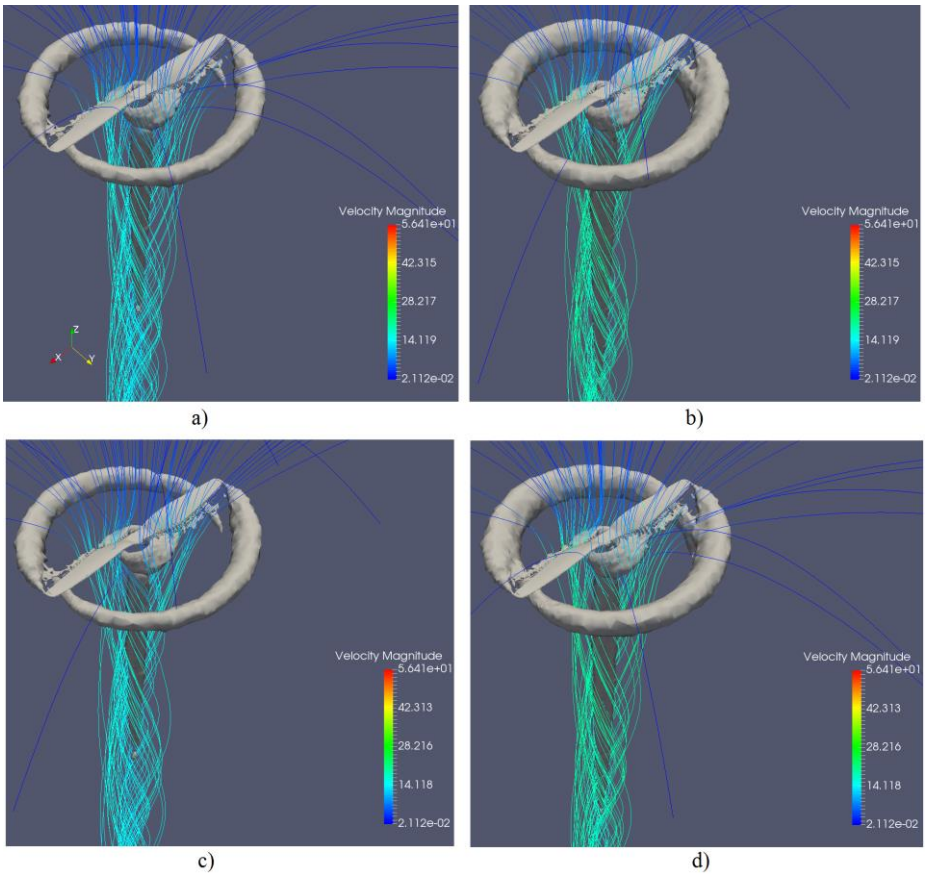

Figure 10. Streamlines colored by velocity magnitude and contours of Q-Criterion= 25000. a) SA 5221RPM, b) SA 6547RPM, c) $k-\omega$ 5221RPM, d) $k-\omega$ 6547RPM.

Figure 10 shows the streamlines colored by velocity magnitude for SA and $k-\omega$ models for 5221 rpm and 6547 rpm. As expected both models increase the magnitude of the velocity down the propeller with the increase of rpm. The streamlines are swirl down around the axis of the propeller.

Figure 11 shows the results for thrust and a comparison with the experimental measures. Both models predict the tendency of thrust, though the differences with the measurements for SA are less than 17.95%, and for $k-\omega$ are around 19.4% for the highest velocities. As seen in figure 10 the predictions of thrust are similar for both models less than 1.26%.

Figure 12 shows the results for torque including the experimental results. Similar to the thrust, the predictions of torque have the same tendency. In this case the differences for the SA predictions and measured are less than 16.5% for the highest velocities. The differences, of the measured torque and the $k-\omega$ results, are less than 16.91% for the highest velocities. The predictions of torque are closer than for thrust, in this case less than 0.46%. The difference with the experimental measurements could be due to the difference of the performance of just one rotor and the performance with the interaction between four rotors and with the fuselage of the drone.

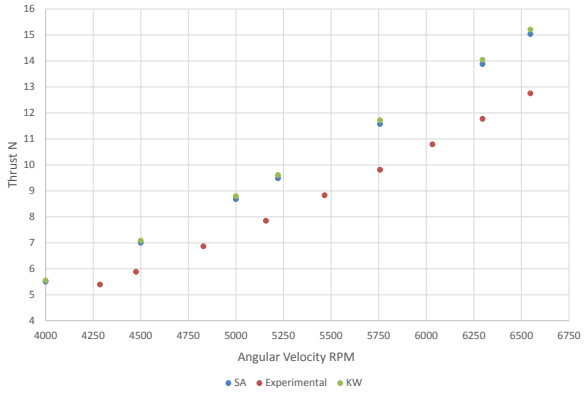

Figure 11. Propeller thrust N.

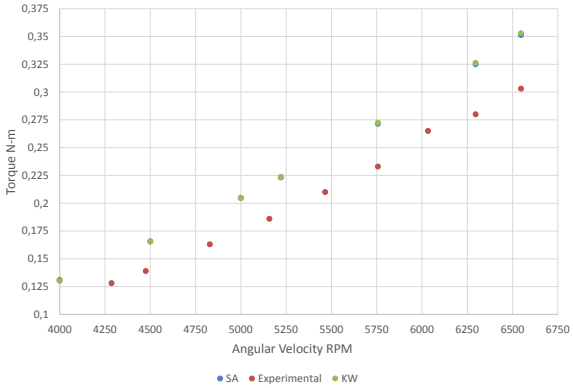

Figure 12. Propeller torque N-m.

The predictions for thrust and torque are closer to the measured for lower rotational velocities and increase with the velocity, see figures 11 and 12, this could be because the diameter of the domain keeps constant, it means that for higher velocities of the propeller could be necessary to increase of the diameter of the domain, but it is necessary to make simulations varying this parameter to support this.

V. Conclusions

A computational model to study the flow around a propeller used in a quad copter was implemented to simulate the behavior of a real propeller at hover condition for a commercial quadcopter of a Colombian company. The models are able to predict the wake, pressure and velocity fields, thrust, torque and performance coefficients of the propeller at different operational rotational velocities using the MRF method in steady state..

Though two different turbulence models were used, the differences are small. The SA and $k-\omega$ models predict basically the same wake for the same angular velocity, when the Q-criterion is used to visualize the main vertical structures. The results of thrust, torque, Cl and Cm for SA and $k-\omega$ are similar but for all cases the $k-\omega$ prediction is higher than the SA results, the difference is less than 1.26% for thrust and 0.46% for torque. Both models overestimate thrust and torque around 18.5% for thrust and 16% for torque in comparision with the experimental results, the differences could be due the interaction of the four rotors between them and also with the fuselage of the aircraft in the experimental measurements. For a better validation of the models is necessary a test bench to a more accurate measurement of thrust and torque.

The main difference found within the two models is in the contours of turbulent viscosity in the far wake, the highest value for the $k-\omega$ model is 2.021×10^{-2} and for the SA model is 5.05×10^{-3}. The $k-\omega$ model predicts a stronger field of turbulent viscosity induced for the propeller, and also a noticeable difference whit the change of velocity, increasing the turbulent viscosity with the increase of velocity. The SA turbulent viscosity field for 5221 rpm and 6547 rpm are similar; it means that in this model the changes of velocity do not have a strong effect on the turbulent viscosity field.

VI. References

1. Kolodny, L.,. Fixed-wing drones not quite taking off in commercial market, a new DroneDeploy study finds. [Online] Crunch Network, 08 15, 2016. [Cited: 09 08, 2016.] https://techcrunch.com/2016/08/15/fixed-wing-drones-not-quite-taking-off-in-commercial-market-a-new-dronedeploy-study-finds/.
2. Hoffmann, G. M., Huang, H., Waslander. S. L., and Tomlin C. J., "Quadrotor Helicopter Flight Dynamics and Control: Theory and Experiment,".. s.l. : American Institute of Aeronautics and Astronautics.
3. Potsdam, M., and Pulliam, T., "Turbulence Modelling Treatment for Rotorcraft Wakes,".. San Francisco CA : Specialist's Conference on Aeromechanics, 2008.
4. Duraisamy, K., and Baeder J. D., "High Resolution Wake Capturing Methodology for Hovering Rotors,".. s.l. : Alfred Gessow Rotorcraft Center, University of Maryland at College Park, 2007.
5. Doerffer, P., and Szulc O., "Numerical Simulation of Model Helicopter Rotor in Hover".. Fiszera : Institute of Fluid-Flow Machinery PAS, 2008.
6. ,". Pandey, K. M., Kumar, D., Das, D., Deka, D., Surana, A., and Das, H. J., "CFD Analysis of an Isolated Main Helicopter Rotor for Hovering Flight. Silchar : IRACST – Engineering Science and Technology: An International Journal, 2011.
7. Yoon, S., Chaderjian, N. M., Pulliam, T. H., Holst, T. L., "Effect of Turbulence Modeling on Hovering Rotor Flows".. Dallas : AIAA Fluid Dynamics Conference, 2015.
8. Gomez, S., Gilkey, L. N., Kaiser, B. E., Poroseva, S. V., “Computational Analysis of a Tip Vortex Structure Shed from a Bio-Inspired Blade.”. Albuquerque : AIAA Aviation, 2014.
9. ”. Lazaro, C. M., and Poroseva, S., “Computational Analysis of the Blade Number Effect on the Performance of a Ducted Propeller. Albuquerque : AIAA SciTech, 2015.
10. Fluent Inc. "FLUENT 6.3 Documentation". [Online] 09 20, 2006. [Cited: 09 20, 2016.] https://www.sharcnet.ca/Software/Fluent6/.
11. Spalart P., and Allmaras S., "A one-equation turbulence model for aerodynamic flows",. s.l. : American Institute of Aeronautics and Astronautics, 1992, Vols. Technical Report AIAA-92-0439.
12. Spalart P. R., and Shur M. L., "On the Sensitization of Turbulence Models to Rotation and Curvature".. 1(5). 297–302., s.l. : Aerospace Sci. Tech., 1997.
13. Wilcox D., "Turbulence Modeling for CFD". C., La Canada, California, : DCW Industries, Inc, 1998.
14. R., Menter F., "Two-Equation Eddy-Viscosity Turbulence Models for Engineering Applications". s.l. : AIAA Journal, 1994, Vols. 32(8):1598-1605,.
15. Smirnov P. E., and Menter F. R., "Sensitization of the SST Turbulence Model to Rotation and Curvature by Applying the Spalart-Shur Correction Term".. Berlin, Germany. : ASME Paper GT, 2008, Vols. 2008-50480.
16. Spakovszky. Z. S. "16.Unified: Thermodynamics and Propulsion". [Online] [Cited: 09 25, 2016.] http://web.mit.edu/16.unified/www/FALL/thermodynamics/notes/node86.html.
17. SAS IP. "Curvature Correction for the Spalart-Allmaras and Two-Equation Models". [Online] ANSYS. [Cited: 09 21, 2016.] https://www.sharcnet.ca/Software/Ansys/16.2.3/en-us/help/flu_th/flu_th_sec_curv_corr.html.